Kovove Mater. 60 2022 171–179
DOI: 10.31577/km.2022.3.171

Influence of spark plasma sintering and conventional sintering on microstructure and mechanical properties of hypereutectic Al-Si alloy and hypereutectic Al-Si/B_4C composites

Melika Ozer[1], Seher Irem Aydogan[2], Alpay Ozer[3]*, Hanifi Cinici[1], Erhan Ayas[4]

[1] *Metallurgical and Materials Engineering, Faculty of Technology, Gazi University, 06560 Ankara, Turkey*
[2] *Metallurgical and Materials Engineering, Institute of Science, Gazi University, 06560 Ankara, Turkey*
[3] *Vocational School of Technical Sciences, Gazi University, 06374 Ankara, Turkey*
[4] *Materials Science and Engineering, Engineering Faculty, Eskişehir Technical University, 26555 Eskişehir, Turkey*

Received 1 February 2022, received in revised form 17 February 2022, accepted 11 May 2022

Abstract

Al-Si compacts and Al-Si/B_4C composites were fabricated by conventional cold pressing + sintering and spark plasma sintering techniques. The effects of powder metallurgy techniques on density, microstructural properties, hardness, and transverse rupture strength were investigated. The advantages of spark plasma sintering, which is one of the fast sintering techniques, over conventional sintering were discussed. Green densities and sintered densities were found to decrease with increasing B_4C addition. The relative density values of the samples produced with spark plasma sintering are over 96 %. B_4C particles were clustered at the grain boundaries of the master alloy and/or in the intergranular pores. An increase of approximately 40 % was determined in the hardness values of the spark plasma sintering samples compared to the cold pressing+sintering samples. Transverse rupture strength was increased in spark plasma sintering samples containing 5 and 10 wt.% B_4C.

K e y w o r d s: aluminum alloys, sintering, microstructure, mechanical properties

1. Introduction

Composites, classified as advanced engineering materials, are attractive materials for modern production technologies due to their advantages, such as high specific strength and high mechanical properties [1–3]. Aluminum and alloy as matrix materials are of great interest in producing metal matrix composites due to their superior properties such as lightness, high specific strength, and good ductility [4, 5]. In this context, hypereutectic Al-Si alloys have grasped the attention of researchers due to their properties, such as high wear resistance, high strength, and low density recently [6–9].

Al-based composites with different chemical compositions are nowadays produced using various powder metallurgy (P/M) techniques [10]. Cold pressing and sintering (CS) is the most widely used conventional P/M technique [11]. In the conventional P/M technique, sintering is a complementary process performed in heat treatment furnaces after the powders are compressed. While acceptable densities can be obtained with this P/M technique, the process is not economical in terms of time and energy. Therefore, energy-saving sintering techniques with reduced sintering times, such as hot press and spark plasma sintering (SPS), have gained importance in recent years. In addition, parts with higher densities can be produced with these techniques [12, 13].

SPS, which is a powder compaction and sintering technique, attracts attention with its fast heating and low sintering temperature. Another interesting advantage of this method is that grain coarsening (growth) does not occur during the sintering process due to the high heating rate [14–17]. In the SPS technique, temperature and compression are applied simultaneously. Prepared powders are charged into graphite dies, and the powders are heated by passing the applied pulsed

*Corresponding author: e-mail address: aozer@gazi.edu.tr

Table 1. Spectral analysis results (wt.%) and powder size distribution of hypereutectic Al-Si powders

		Al	Si	Cu	Mg	Lubr. Amidwax
Alumix 231®	Production method: Gas atomization	Remainder	15.36	3.155	0.58	1.5
		Powder size distribution				
		D_{50} ≈ 75		D_{10} ≈ 22		D_{90} ≈ 190

Table 2. Conventional P/M and SPS process parameters

Conventional P/M (Cold pressing + sintering)	Sintering pressure (MPa)	Sintering temperature (℃)	Sintering time (min)	Heating rate (℃ min^{-1})	Sintering atmosphere	Eliminate the lubricant
	620	555	60	5	N_2	400 ℃ for 20 min
Spark plasma sintering	50	450	5	100	Vacuum	

Table 3. Specimen codes and applied processes

Specimen Notation	Materials	Sintering	Sintering temperature (℃)	Sintering time (min)
CS-555	Alumix 231®	Conventional	555	60
5-CS-555	Alumix 231® + 5 wt.% B_4C	Conventional	555	60
10-CS-555	Alumix 231® + 10 wt.% B_4C	Conventional	555	60
15-CS-555	Alumix 231® + 15 wt.%B_4C	Conventional	555	60
SPS-450	Alumix 231®	Spark Plasma	450	5
5-SPS-450	Alumix 231® + 5 wt.% B_4C	Spark Plasma	450	5
10-SPS-450	Alumix 231® + 10 wt.% B_4C	Spark Plasma	450	5
15-SPS-450	Alumix 231® + 15 wt.% B_4C	Spark Plasma	450	5

direct current over the powders. The formation of arc points between the powder particles during the process facilitates sintering. As a result, homogeneously sintered samples with improved mechanical properties are produced [18–20].

In the present work, hypereutectic Al-Si alloy powders were chosen as the matrix material. Boron carbide particles in the B_4C composition were used as reinforcement. Al-Si compacts and Al-Si/B_4C composites were fabricated by conventional P/M (cold pressing+sintering) and SPS techniques. The effects of P/M techniques on density, microstructural properties, hardness, and transverse rupture strength were investigated. The advantages of SPS, which is one of the fast sintering techniques, over conventional sintering are discussed.

2. Materials and methods

Al-Si compacts and Al-Si/B_4C composites were fabricated using CS and SPS techniques. Hypereutectic Al-Si powders (Ecka Alumix 231®) were used as metal matrix. Spectral analysis results and powder size distribution of hypereutectic Al-Si powders are given in Table 1. B_4C particles with a density of 2.52 g cm^{-3} and (D_{50}) 10 μm average particle size were used as reinforcement in the fabrication of composites.

For the production of Al-Si/B_4C composites, the reinforcing element was added to the matrix material at the rate of 5, 10, and 15 wt.%. Prepared powders were mixed in a triaxial mixer for 45 min to obtain a homogeneous mixture. Conventional P/M and SPS process parameters are given in Table 2. For SPS, 25 g powder was charged to the die, and a preload of 1 MPa was applied. Table 3 illustrates the specimen notations of the samples.

The densities of green, CS, and SPS samples were measured by Archimedes' technique according to ASTM B962-08. The densities were reported as % of the relative density (% RD) proportional to the theoretical density value. The theoretical densities were calculated by the rule of mixtures using material com-

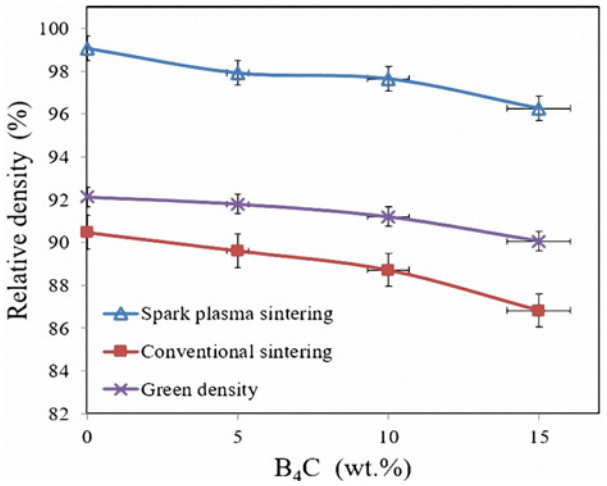

Fig. 1. Density variation with wt.% B_4C particle ratio and sintering technique.

position. Samples were subjected to standard metallographic processes for microstructure analysis. Keller's etching was used for etching the samples. An optical microscope (Leica DMI 5000 M) and scanning electron microscope (SEM) (Jeol JSM 6060 LV) were used for microstructure analysis. Hardness tests of the samples were performed using the Brinell hardness method with 31.5 kgf load and 2.5 mm ball diameter. Three-point bending tests were carried out on the samples according to the ASTM-B528-16. The tests were performed at a feed rate of 1 mm min^{-1}. Also, the transverse rupture strength (TRS) values of the samples were calculated using the BlueHill program.

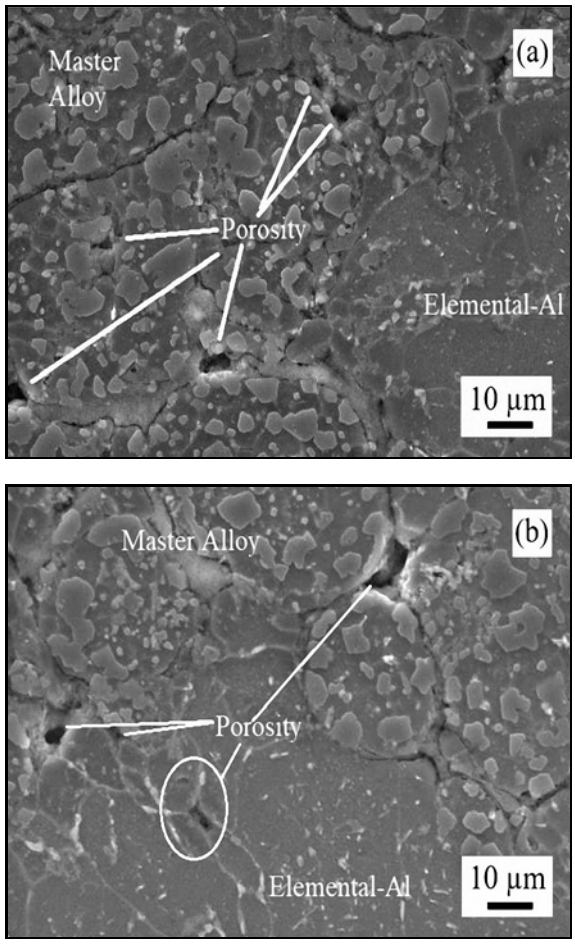

Fig. 2. SEM micrographs of samples: (a) Green Al-Si and (b) CS-555.

3. Results and discussion

3.1. Density

The change in density of the samples according to the B_4C particle ratio and P/M technique is given in Fig. 1. The green densities and sintered densities of the samples decreased with increasing B_4C addition. This decrease is attributed to the pores between the matrix powder grains with B_4C particles and between the clustered B_4C particles.

The remarkable result in the graph given in Fig. 1 is that the density values of the samples produced with CS are lower than the green density values. Studies on hypereutectic Al-Si alloys mention the existence of a liquid phase [21–24]. It has been reported in the literature that the liquid phase begins to form at about 500–525 ℃ [24–28]. Since no pressure is applied during sintering in the traditional sintering technique, the liquid phase formed is collected locally and causes sudden dimensional changes. It has been reported that large pores are formed in the microstructure due to a rapid condensation period and solidification of the liquid phase during the cooling process [22, 24, 29]. These events occurring in the microstructure during cooling caused lower densities to be obtained by conventional sintering. When the micrographs in Fig. 2 are examined, it is seen that pores are formed in the master alloy grains and elemental Al grains in both the green Al-Si sample and the CS-555 sample. While pores in green samples are formed due to conventional P/M process mechanics, the formation of pores in the CS sample is attributed both to the nature of the P/M technique and to the liquid phase caused by Al-Si, Al-Cu, and Al-Mg eutectics [23, 26, 30].

SPS is a pressure sintering technique. It is a technique performed at lower temperatures than conventional sintering. The formation of sparks at the contact points or gaps between the powders charged to the die in SPS causes instantaneous local high temperatures. With the sudden regional temperature increase, evaporation and melting take place on the surfaces of the powder grains. Neck regions are formed around the contact area of the grains where melting occurs

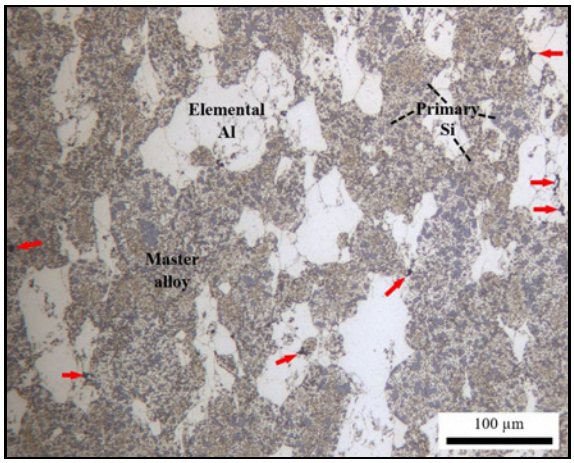

Fig. 3. Optical micrograph of no etching SPS-450 sample (light dark particles in the master alloy are primary Si particles).

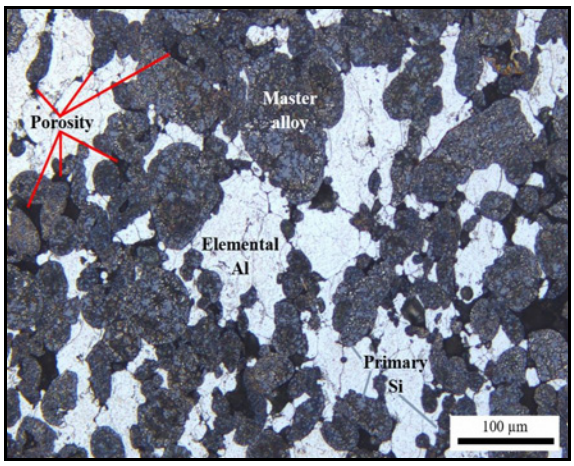

Fig. 4. Optical micrograph of the green hypereutectic Al-Si alloy.

[31]. In addition, micro-spaces between powder grains and/or B_4C clusters are eliminated and/or minimized by the effect of applied pressure. Moreover, the high electrical discharge that occurs at the powder grain contact points during SPS creates a cleaning effect on the surfaces of the powder grains, increasing grain-border diffusion [19]. Thanks to these advantages provided by the SPS technique, high-density values were obtained in this study. An optical micrograph of the no etching SPS-450 sample is given in Fig 3. When the micrograph is examined, it is seen that the amount of porosity is quite low, and the porosity size is small (pores are indicated by arrows, and the amount of porosity is about 0.92 %).

3.2. Microstructure

In Fig. 4, an optical micrograph of green hypereutectic Al-Si alloy is given. The microstructure consists of master alloy (Al-, Si-, Cu- and Mg-rich), elemental Al, and primary Si particles (grayish in color in the master alloy grains). It was observed that the pores in the microstructure were concentrated around the master alloy grains.

Optical micrographs of hypereutectic Al-Si compacts and hypereutectic Al-Si/B_4C composites produced with CS and SPS are given in Fig. 5. Since the CS process was carried out at 555 °C, more pores were formed in the microstructure than SPS with the effect of the liquid phase formed. In addition, the pressure applied in the SPS caused the closure of the micropores and thus an increase in the density.

When the micrographs of Figs. 5a–d were examined, it was determined that B_4C particles clustered at the grain boundaries of the master alloy and/or in the intergranular spaces. In addition, it is seen that the interfacial bond between the master alloy grains and between the master alloy grains and B_4C particles is not formed and/or partially formed. The high surface tension of B_4C ceramic particles and the poor wettability of the B_4C particles of the liquid phase formed at sintering temperatures can be said to be the reason for this negativity. It was determined that the amount and size of the pores increased with increasing wt.% B_4C addition. The increase in porosity with increasing B_4C addition is attributed to incompatibility between matrix grains and B_4C particles. The incompatibility between the matrix grains and the B_4C particles prevents the formation of a continuous and effective interface. Micrographs of the SPS samples given in Figs. 5e–h gave similar images. Due to the advantages of the SPS technique, microstructures with less porosity were obtained in the samples produced with the SPS technique. However, with increasing wt.% B_4C amount, the porosity increased in SPS samples as well. With increasing wt.% B_4C, B_4C clusters were formed, which caused the pores to become larger and the number of pores to increase. In addition, when the micrographs given in Figs. 5a–h are examined, it is seen that the B_4C particle size also affects the size of the pores. Namely, as the B_4C particle size increased, larger pores were formed in the regions where these particles were found.

SEM images of 15-CS-555 and 15-SPS-450 samples are given in Fig. 6. The presence of large pores is evident in the micrograph of the 15-CS-555 sample for the regions of B_4C particles. In addition, after sintering, bonding problems are seen between the master alloy grains and/or between the master alloy/elemental Al grains. In the 15-SPS-450 sample, better bonds were formed between the grains. In addition, it can be said that a good interface is formed between the B_4C particles and the matrix grains compared to the 15-CS--555 sample. Obtaining a more homogeneous and acceptable microstructure in the 15-SPS-450 sample is

related to the process parameters, especially the applied pressure. The pressure applied during the process reduced the size of the pores between both the matrix grains and the matrix grains/B_4C. This effect causes the closure of the pores and/or the reduction of the size of the pores. In addition, with the effect of applied pressure, the diffusion mechanism becomes more effective, and a good interface is formed.

3.3. Hardness

The change in hardness with the B_4C particle ratio of the samples produced with CS and SPS is given in Fig. 7. Consistent with the density data, SPS samples yielded higher hardness values. Compared to CS samples, the hardness values of SPS samples are approximately 40 % higher. The good bonding between

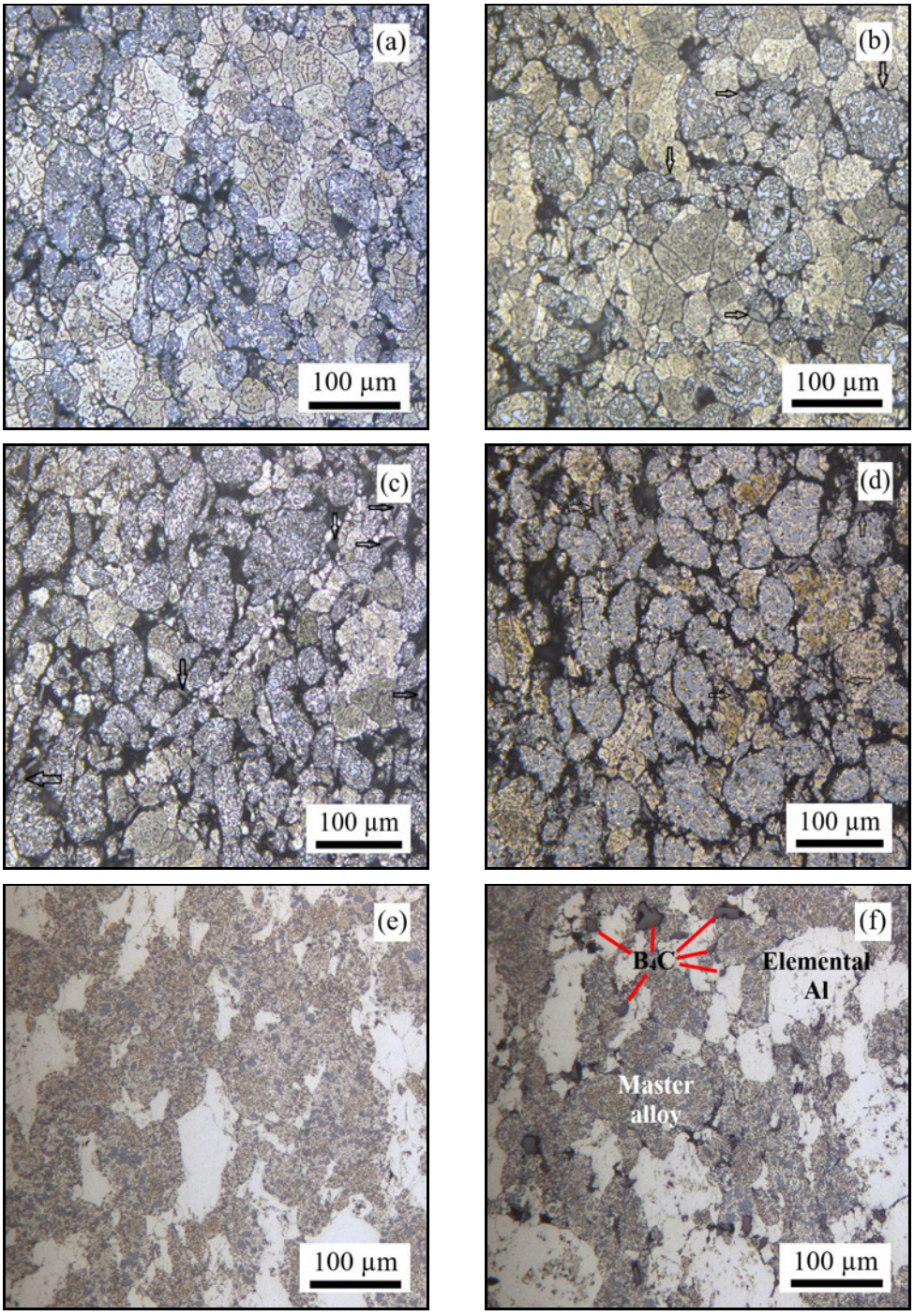

Fig. 5a–f. Optical micrographs of hypereutectic Al-Si compacts and Al-Si/B_4C composites produced with CS and SPS: (a) CS-555, (b) 5-CS-555, (c) 10-CS-555, (d) 15-CS-555, (e) SPS-450, (f) 5-SPS-450.

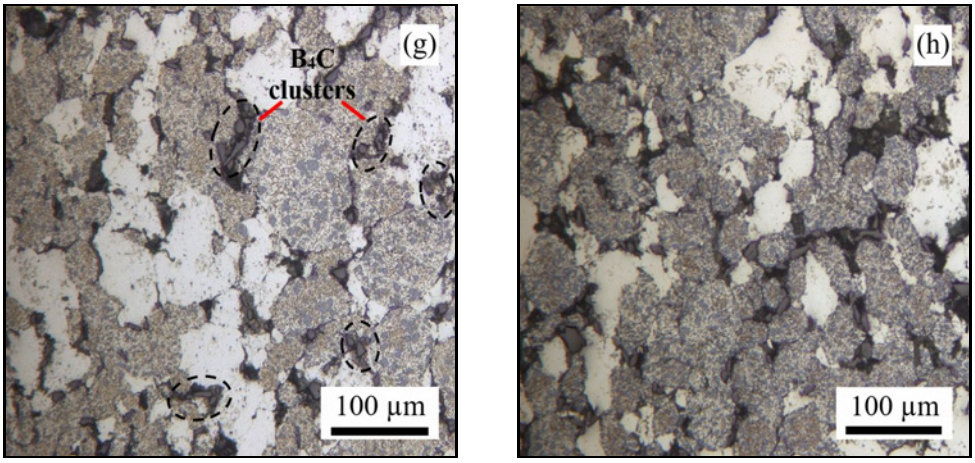

Fig. 5g,h. Optical micrographs of hypereutectic Al-Si compacts and Al-Si/B_4C composites produced with CS and SPS: (g) 10-SPS-450, and (h) 15-SPS-450.

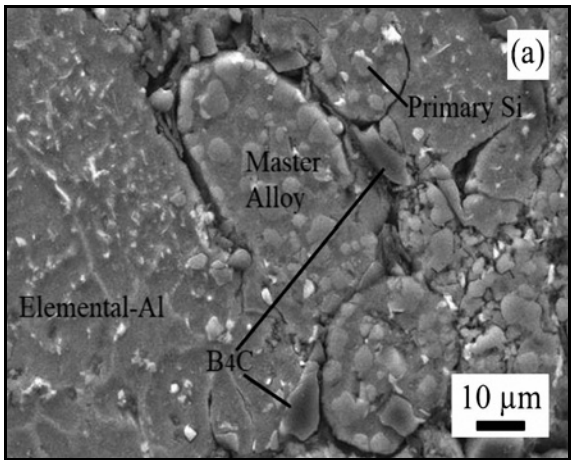

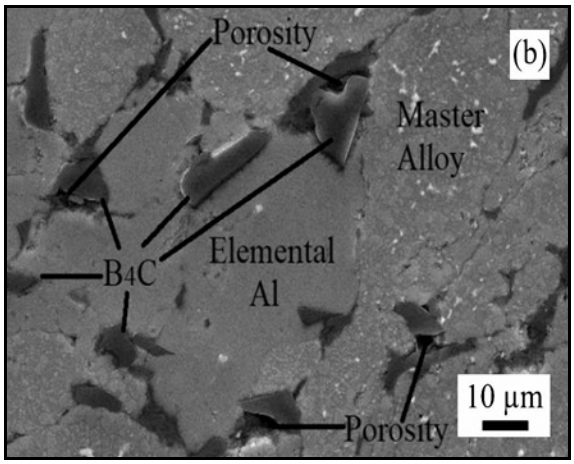

Fig. 6. SEM micrographs: (a) 15-CS-555 and (b) 15-SPS--450.

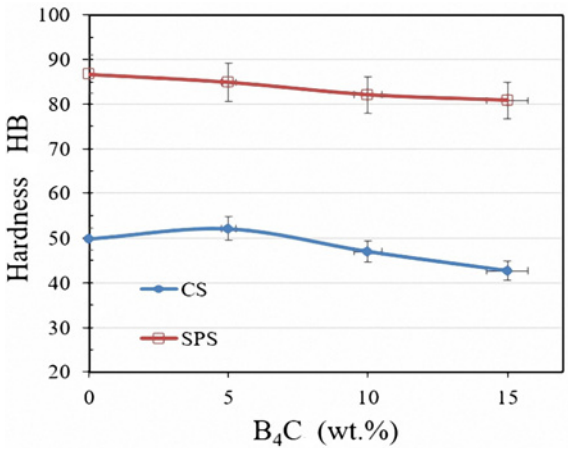

Fig. 7. The effects of wt.% B_4C particle ratio on hardness in samples produced with CS and SPS.

the powder grains and the low amount of pores in the SPS samples caused the density and hardness values to be higher than those of the CS samples. Increasing B_4C addition caused a decrease in the hardness value of the samples. Nevertheless, the decrease in hardness was limited to ∼5 %. An increase in hardness can be expected with increasing B_4C addition. However, B_4C addition to the microstructure causes porosity between the matrix grains and B_4C and/or B_4C clusters. The increased porosity in the microstructure with the addition of B_4C is the reason for the decrease in hardness. An increase of approximately 3 % was detected only in the 5-CS-555 sample. This result can be explained as the addition of 5 wt.% B_4C particles has a greater effect on hardness than the porosity.

3.4. Three-point bending test

The TRS values of the samples according to the wt.% of the B_4C particle ratio and the P/M technique are given in Fig. 8. Very high TRS values were determined in SPS samples compared to CS samples. This is attributed to the porosity in the microstructure, the bonding between the matrix grains, and the

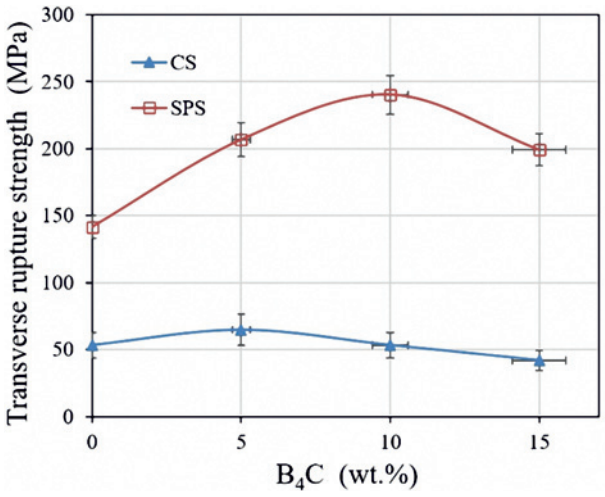

Fig. 8. Variation of TRS with wt.% B_4C particle ratio in samples produced with CS and SPS.

interface between the matrix grains/B_4C particles. In accordance with the hardness, an increase of approximately 14 % was observed in the TRS value of the 5-CS-555 sample. The increased porosity with the increasing B_4C particle addition caused a decrease in the TRS values of the 10-CS-555 and 15-CS-555 samples.

When the TRS values of the samples produced with the SPS technique were examined, it was determined that the TRS values increased with the addition of 5 and 10 wt.% B_4C. An increase of approximately 32 % was detected in the 5-SPS-450 sample, and a further 14 % increase was determined in the 10--SPS-450 sample. In addition to the matrix reinforcing feature of B_4C particles, preventing the movement of grain boundaries and thus restricting the plastic flow of the matrix are reasons for these increases. Increasing the amount of B_4C by weight from 5 to 10 % further strengthened this effect, reducing the distance between particles. However, the increase in the 10-SPS--450 sample was less than the increase in the 5-SPS--450 sample. This was attributed to an increase in the number and size of B_4C clusters with increasing wt.% B_4C content. The increase in the number and size of B_4C clusters also resulted in an increase in the size and number of pores. Increasing the wt.% B_4C amount to 15 % caused a decrease of approximately 17 % in TRS value compared to the 10-SPS-450 sample. As can be seen in the micrograph in Fig. 5h, with the addition of 15 wt.% B_4C, the densely observed B_4C clusters and coarse porosity in the microstructure caused a decrease in TRS in this sample.

4. Conclusions

The results of this study are summarized below:

– Green densities and sintered densities were decreased with increasing B_4C particle addition.

– The relative density values of the samples produced with SPS are over 96 %. The highest relative density value of 99.08 % was obtained in the hypereutectic Al-Si sample, which did not contain B_4C.

– An increase of approximately 40 % was determined in the hardness values of the SPS samples compared to the CS samples.

– Increasing B_4C addition caused a decrease in the hardness value of the samples. This decrease in hardness is restricted to ∼5 %.

– TRS values were increased in SPS samples containing 5 and 10 wt.% B_4C particles. On the other hand, in SPS samples containing 15 wt.% B_4C particles, a decrease of approximately 17 % was determined in TRS values compared to the 10-SPS-450 sample. However, over 150 % increase was determined in TRS values of SPS samples compared to CS samples.

– When B_4C added hypereutectic Al-Si alloys are produced with the SPS technique, there is no improvement in hardness value. However, a significant increase in TRS values (approximately min 29 % to max 46 %) is observed. Therefore, hypereutectic Al-Si/B_4C composites produced by the SPS technique can be used in parts exposed to compression stress.

– As a result, P/M samples produced by the SPS technique showed better microstructures and mechanical properties than the CS technique. In addition, the fact that the sintering temperature and holding time in the SPS technique are much lower than those in the CS technique, so it offers significant advantages in terms of energy and time savings.

Acknowledgement

This work has been supported by Gazi University Scientific Research Projects Coordination Unit under grant number 07/2019-13.

References

[1] I. A. Ibrahim, F. A. Mohamed, E. J. Lavernia, Particulate reinforced metal matrix composites – A review, J. Mater. Sci. 26 (1991) 1137–1156. https://doi.org/10.1007/BF00544448

[2] V. Khanna, V. Kumar, S. A. Bansal, Mechanical properties of aluminium-graphene/carbon nanotubes (CNTs) metal matrix composites: Advancement, opportunities and perspective, Mater. Res. Bull. 138 (2021) 111224. https://doi.org/10.1016/j.materresbull.2021.111224

[3] D. Kumar, R. K. Phanden, L. Thakur, A review on environment friendly and lightweight magnesium-based metal matrix composites and alloys, Mater. Today – Proc. 38 (2021) 359–364. https://doi.org/10.1016/j.matpr.2020.07.424

[4] V. Puchy, M. Podobova, R. Dzunda, P. Hvizdos, O. Velgosova, M. Besterci, B. Ballokova, Graphene nanoplatelets reinforced aluminum alloy matrix composites produced by spark plasma sintering, Kovove Mater. 59 (2021) 237–244. https://doi.org/10.4149/km_2021_4_237
[5] Y. Kaplan, S. Aksöz, H. Ada, E. İnce, S Özsoy, The effect of aging processes on tribo-metallurgy properties of Al based ternary alloys product by P/M technique, Sci. Sinter. 52 (2020) 445–456. https://doi.org/10.2298/SOS2004445K
[6] W. G. E. Mosher, G. J. Kipouros, W. F. Caley, I. W. Donaldson, D. P. Bishop, On hot deformation of aluminium-silicon powder metallurgy alloys, Powder Met. 54 (2011) 366–375. https://doi.org/10.1179/003258910X12678035166773
[7] J. Zeng, C. Zhu, W. Wang, X. Li, H. Li, Evolution of primary Si phase, surface roughness and mechanical properties of hypereutectic Al-Si alloys with different Si contents and cooling rates, Phil. Mag. Lett. 100 (2020) 581–587. https://doi.org/10.1080/09500839.2020.1824081
[8] F. K. Charandabi, H. R. Jafarian, S. Mahdavi, V. Javaheri, A. Heidarzadeh, Modification of microstructure, hardness, and wear characteristics of an automotive-grade Al-Si alloy after friction stir processing, J. Adhes. Sci. Technol. 35 (2021) 2696–2709. https://doi.org/10.1080/01694243.2021.1898858
[9] T. T. Saravanana, M. Kamaraj, S. C. Sharma, S. Anoop, S. K. Manwatkar, K. V. Ravikanth, A. Venugopal, S. Kumaran, Influence of characteristic eutectic free microstructure on mechanical and corrosion response of spark plasma sintered hypereutectic Al-Si alloy, Mater. Lett. 308 (2022) 131104. https://doi.org/10.1016/j.matlet.2021.131104
[10] S. C. Tjong, Z. Y. Ma, Microstructural and mechanical characteristics of in situ metal matrix composites, Mat. Sci. Eng. R: Reports 29 (2000) 49–113. https://doi.org/10.1016/S0927-796X(00)00024-3
[11] J. W. Kaczmar, K. Pietrzak, W. Wlosinski, The production and application of metal matrix composite materials, J. Mater. Process. Tech. 106 (2000) 58–67. https://doi.org/10.1016/S0924-0136(00)00639-7
[12] U. C. Oliver, A. V. Sunday, E. I. I. Christain, M. M. Elizabeth, Spark plasma sintering of aluminium composites – A review, Int. J. Adv. Manuf. Technol. 112 (2021) 1819–1839. https://doi.org/10.1007/s00170-020-06480-7
[13] V. L. Arantes, J. Sakihama, J. Vleugels, Spark plasma sintered step graded Al_2O_3-NbC composites, Ceram. Int. 47 (2021) 19481–19488. https://doi.org/10.1016/j.ceramint.2021.03.285
[14] R. Yamanoğlu, W. L. Bradbury, E. A. Olevsky, R. M. German, Comparative evaluation of densification and grain size of ZnO powder compacts during microwave and pressureless spark plasma sintering, Adv. Appl. Ceram. 111 (2012) 422–426. https://doi.org/10.1179/1743676112Y.0000000017
[15] V. Puchy, J. Kovacik, A. Kovalcikova, R. Sedlak, R. Dzunda, J. Dusza, L. Falat, M. Podobova, M. Besterci, P. Hvizdos, Mechanical and tribological properties of TiB_2-Ti composites prepared by spark plasma sintering, Kovove Mater. 57 (2019) 435–442. https://doi.org/10.4149/km_2019_6_435
[16] V. Mamedov, Spark plasma sintering as advanced PM sintering method, Powder Metall. 45 (2002) 322–328. https://doi.org/10.1179/003258902225007041
[17] A. Nisar, C. Zhang, B. Boesl, A. Agarwal, Unconventional materials processing using spark plasma sintering, Ceramics 4 (2021) 20–39. https://doi.org/10.3390/ceramics4010003
[18] M. Omori, Sintering, consolidation, reaction and crystal growth by the spark plasma system (SPS), Mat. Sci. Eng. A – Struct. 287 (2000) 183–188. http://dx.doi.org/10.1016/S0921-5093(00)00773-5
[19] Z. Shen, M. Johnsson, Z. Zhao, M. Nygren, Spark plasma sintering of alumina, J. Am. Ceram. Soc. 85 (2002) 1921–1927. https://doi.org/10.1111/j.1151-2916.2002.tb00381.x
[20] D. Ghahremani, T. Ebadzadeh, A. Maghsodipour, Spark plasma sintering of mullite: Relation between microstructure, properties and spark plasma sintering (SPS) parameters, Ceram. Int. 41 (2015) 6409–6416. https://doi.org/10.1016/j.ceramint.2015.01.078
[21] M. Ozer, S. I. Aydogan, H. Cinici, A. Ozer, Effects of sintering techniques and parameters on microstructure and mechanical properties of Al-15Si-2.5Cu-0.5Mg compacts and Al-15Si-2.5Cu-0.5Mg/B_4C composites, Materials Today Communications 30 (2022) 103192. https://doi.org/10.1016/j.mtcomm.2022.103192
[22] D. W. Heard, I. W. Donaldson, D. P. Bishop, Metallurgical assessment of a hypereutectic aluminum-silicon P/M alloy, J. Mater. Process. Tech. 209 (2009) 5902–5911. https://doi.org/10.1016/j.jmatprotec.2009.07.007
[23] H. Rudianto, S. Yang, K. Nam, Y. Kim, Mechanical properties of Al-14Si-2.5Cu-0.5Mg aluminum-silicon P/M alloy, Rev. Adv. Mater. Sci. 28 (2011) 145–149.
[24] S. S. Su, I. T. H. Chang, W. C. H. Kuo, Effects of processing conditions on the sintering response of hypereutectic Al-Si-Cu-Mg P/M alloy, Mater. Chem. Phys. 139 (2013) 775–782. https://doi.org/10.1016/j.matchemphys.2013.02.031
[25] A. Ozer, The microstructures and mechanical properties of Al-15Si-2.5Cu-0.5Mg/(wt.%)B_4C composites produced through hot pressing technique and subjected to hot extrusion, Mater. Chem. Phys. 183 (2016) 288–296. https://doi.org/10.1016/j.matchemphys.2016.08.029
[26] T. Schubert, T. Weissgaerber, B. Kieback, H. Balzer, H. C. Neubing, U. Baum, R. Braun, Aluminium PM 'is a challenge that industry can overcome', Metal Powder Report V 60 (2005) 32–34, 37. https://doi.org/10.1016/S0026-0657(05)00370-X
[27] I. Arribas, J. M. Martin, F. Castro, The initial stage of liquid phase sintering for an Al-14Si-1.5Cu-0.5Mg (wt.%) P/M alloy, Mat. Sci. Eng. A – Struct. 527 (2010) 3949–3966. https://doi.org/10.1016/j.msea.2010.02.078
[28] Z. Cai, C. Zhang, R. Wang, C. Peng, X. Wu, Effect of copper ctontent on microstructure and mechanical properties of Al/Sip composites consolidated by liquid phase hot pressing, Mater. Design 10 (2016) 10–17. https://doi.org/10.1016/j.matdes.2016.07.085
[29] E. Crossin, J. Y. Yao, G. B. Schaffer, Swelling during liquid phase sintering of Al-Mg-Si-Cu alloys, Powder

Metall. 50 (2007) 354–358.
https://doi.org/10.1179/174329007X223947

[30] W. Judge, G. Kipouros, Powder Metallurgy Aluminum Alloys: Structure and Porosity, In: G. E. Totten, M. Tiryakioglu, O. Kessler (Eds.), Encyclopedia of Aluminum and Its Alloys, CRC Press Taylor & Francis Group, New York 2018, pp. 1977–1995. https://doi.org/10.1201/9781351045636

[31] N. Saheb, Z. Iqbal, A. Khalil, A. S. Hakeem, N. A. Aqeeli, T. Laoui, A. Al-Qutub, R. Kirchner, Spark plasma sintering of metals and metal matrix nanocomposites: A review, J. Nanomater. (2012) 983470. https://doi.org/10.1155/2012/983470